Surface tension of amorphous polymer films

Thorsten Hapke, Gerald Pätzold, and Dieter W. Heermann*

Institut für Theoretische Physik, Universität Heidelberg, Philosophenweg 19, D–69120 Heidelberg, Germany and Interdisziplinäres Zentrum für wissenschaftliches Rechnen der Universität Heidelberg

(February 10, 1998)

Abstract

We study the surface tension for thin, amorphous polymer films by means of computer simulation. In the framework of molecular dynamics, we present surface tension measurements via the fluctuation spectrum of capillary waves in the long-wavelength limit. This approach uses arguments from continuum mechanics and for sufficiently large systems, we find good agreement with of the theory. In addition, we observe the spreading of the surface thickness with increasing lateral system size, an effect which allows another estimate of the surface tension. Furthermore we studied the correlation between the two surfaces and measured the transverse length scale by varying the film thickness. Finally we looked at the temperature dependence the bulk density in the center of the polymer film, and the thickness of the surface region in the regime above the glass transition temperature but significantly below the critical temperature.

Keywords: Polymer surfaces; computer simulation; surface tension; capillary

*Contact: heermann@tphys.uni-heidelberg.de, http://wwwcp.tphys.uni-heidelberg.de/

waves.

68.10.Cr, 68.60.-p

Typeset using REVTEX

INTRODUCTION

Thin films and their surface properties play an important role in numerous technological applications of polymers. Film geometry is essential to lubrication, in thermoplastic processing, foil manufacturing, and in using polymers as adhesives. Experimental and manufacturing techniques advance to smaller and smaller scales and it is not just the bulk behavior that decides about the technological applicability of a certain material but also its surface properties.

In this context, the determination of the surface tension is of particular interest, and a number of recent publications [1–5] is devoted to this for the case of polymers. To compute the surface tension γ, many authors take the virial route based on the Fowler approximation [6]. This results in the Kirkwood-Buff formula,

$$\gamma = \frac{1}{4} \int_{\infty}^{+\infty} dz_1 \int dr_{12} \left(r_{12} - \frac{3z_{12}^2}{r_{12}} \right) u'(r_{12}) \rho^{(2)}(r_1, r_2) \,, \tag{1}$$

where r_{12} is the distance between molecules 1 and 2, $\rho^{(2)}$ is the generalized density, and u' is the derivate of the interaction potential. The same expression can be obtained starting with the components of the pressure tensor [7]. Adapting Eqn. (1) for numerical evaluation in computer simulation leads to

$$\gamma = \frac{1}{A} \left\langle \sum_{i<j} \left(r_{ij} - \frac{3z_{ij}^2}{r_{ij}} \right) u'(r_{ij}) \right\rangle \,, \tag{2}$$

where the summation is taken over all pairs of molecules in a sampling area A which has to be parallel to the xy-coordinate plane. The brackets denote the thermal average over the entire simulation.

Unfortunately, the Kirkwood-Buff relation, Eqn. (1), leads to restricted accuracy even for Lennard-Jones fluids [8]. One reason for this is the omission of three-body interactions [9,10]. Especially for macromolecules this defect will be a serious one and it is difficult to devise a correction scheme. Another source of inaccuracies are capillary waves, which cause fluctuations over a wide range. With the enlargement of the system their amplitudes

grow (which means, from a practical point of view, we cannot profit from self-averaging by just simulating larger systems). One could think of setting up local coordinate frames (like in Fig. 1) such that the z' direction is always perpendicular to the surface, and to evaluate the Kirkwood-Buff formula in these local frames. However, due to the coarseness of our raw data (monomer positions etc.) such an approach seems to be too delicate to implement at the moment.

FIGURES

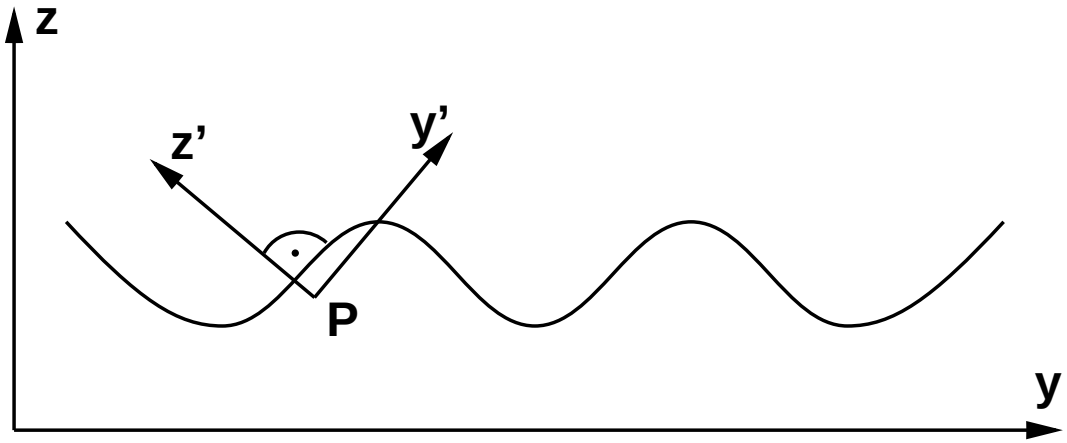

FIG. 1. Sketch of surface with capillary waves. The Kirkwood-Buff relation assumes a planar surface. The existence of capillary waves limits the accuracy of measurements received from this method. To increase the accuracy local coordinate systems may have to be implemented.

To circumvent these problems we take a route over a more macroscopic point of view and use the fluctuation spectrum of the capillary waves to determine the interface tension. The work [11,12] already succeeded in applying this method to compute the surface tension between two highly incompatible polymers on the lattice using the bond fluctuation model (for that model, see e.g. Ref. [13]).

POLYMER MODEL AND SIMULATION PROCEDURE

For the polymer chains, we use a united atom model in conjunction with Newtonian dynamics. In addition to harmonic chain forces which keep the bond lengths next to the equilibrium value, we model the fluctuation of bond angles, again by a quadratic potential. Between monomers which do not participate in mutual bond length or bond angle interactions, Lennard–Jones forces are acting. Note that we neglect any torsional potential in the present study. To be explicit, the Hamiltonian of the model is of the form

$$H = H_{\mathrm{bondlength}} + H_{\mathrm{bondangle}} + H_{\mathrm{LJ}} \,,$$

$$H_{\mathrm{bondlength}} = \sum_{\mathrm{bonds}} \frac{k_b}{2} \left(l_{\mathrm{bond}} - l_0 \right)^2 \,,$$

$$H_{\mathrm{bondangle}} = \sum_{\mathrm{angles}} \frac{k_\theta}{2} \left(\cos\theta_{\mathrm{angle}} - \cos\theta_0\right)^2 , \tag{3}$$

$$H_{\mathrm{LJ}} = \sum_{\substack{\mathrm{pairs\ of} \\ \mathrm{monomers}}} 4\epsilon \left[\left(\frac{\sigma}{r_{\mathrm{pair}}}\right)^{12} - \left(\frac{\sigma}{r_{\mathrm{pair}}}\right)^{6} \right] .$$

The Lennard–Jones interaction is implemented with a cutoff of $2.5\,\sigma$ and appropriate potential shifts are used to retain continuity. We use molecular dynamics methods to compute the motion of the monomers. Models of this kind are described at various places in the literature (for an introduction, refer to Ref. [14]). We intend to capture some essential features of polyethylene chains and appropriate model parameters are compiled in Tab. I (see also Refs. [15–18]).

Simulations to probe the surface properties and their dependence on the system size were typically performed at the reduced temperature $T^* = T/(\epsilon/k_{\mathrm{B}}) = 6.0$ (referring to Tab. I, this corresponds to about 360 Kelvin). At this temperature, the model behaves in a number of aspects like a liquid, but we are still well below the Θ-point. To study the influence of temperature, runs were made from $T^* = 3$ to $T^* = 10$. We stress that our simulations are not supposed to fully mimic real polyethylene (it has been demonstrated, however, that much can be achieved by carefully tuning the parameters of united atom models [16]). The chain lengths are still too short and we treat chain–end monomers like mid–chain monomers. We also neglect the torsional potential (the rotation about C–C axes is not restricted). The high temperature helps to ensure that in feasible simulation times, the chains travel several radii of gyration in order to guarantee correct thermodynamic properties.

To prepare amorphous polymer surfaces like the one in Fig. 2, we start from a homogeneous configuration with periodic boundary conditions in all space directions. The monomer number density in the system is chosen to be comparable to that of real polyethylene, i.e. $\rho^* = 2.0$ corresponding to a mass density of $\rho = 0.86$ g/ccm. This system is first run through some relaxation phase such that all chains have diffused over a distance of at least two radii of gyration. Thereafter, the extension of the simulation box in the z-direction is tripled which allows to model a freely standing film retaining all periodic boundary conditions. In

a subsequent second relaxation phase, the density profile across the surface, see e.g. Fig. 5, quickly approaches its stationary shape, independent of the initial density in the fully filled periodic box. The bulk density in the center of the film is mainly determined by the chain length and the cutoff radius used to truncate the Lennard-Jones interaction in the computer simulation. We have already reported on this and other phenomena (like the chain-end distribution and the orientation of the chain end-to-end vectors) observed in simulations of freely standing films in considerable detail [18].

FIG. 2. Freely standing polymer film. The monomers are represented by spheres using their Lennard-Jones length $\sigma = 3.8$ Å as the radius. The horizontal extension of the film is 60 Å times 180 Å, the vertical thickness is about 75 Å.

Since we have to treat at least 8000 interacting particles to produce reasonable results, advanced simulation techniques must be employed. Besides the well-known Verlet-table method [14], we use the linked-cell algorithm [19]. Then, as reported in Tab. II, the computational time grows linearly with the particle number as long as sufficient memory is available.

Because the simulated film has two surfaces which we want to analyze simultaneously, we measure the positive distance between points on the surfaces and the lateral plane through the film's center of mass. There are several ways to actually sample the surfaces. One may think of setting up a Voronoi diagram, or a Delauny triangulation, respectively [20], and to identify the outermost layers. The input parameter required would be the maximum distance between next neighbors. However, this approach is difficult to program and also lengthly to compute. An approximate, but feasible way is to divide the film (by use of a regular grid in

a lateral plane) into a number of columns, i.e. to cover the surface by a number of patches. Within each patch we identify the monomer with the extremal z–coordinate. Doing so, we obtain a mapping from the patches to a set of height values. In the course of the work, it turns out to be advantageous to average over three extremal monomers in each patch to obtain smoother results without loosing information.

It has been checked that the long wave length results from the subsequent two-dimensional Fourier transform of the height function do not depend on the grid parameter used to define the surface patches. However, for a properly chosen resolution, sampling errors can be reduced significantly. A grid parameter which corresponds to the hardcore radius of the monomers is recommended.

THEORETICAL BACKGROUND

Surfaces and interfaces in polymer systems possess a finite width. One hereby has to distinguish between the "intrinsic" width (due to the chain connectivity) and the width observed because of capillary waves. The latter stems from taking a time-, space-, or ensemble-averaged look at a vibrating, thermally excited surface (which could, in principle, locally show a sharp intrinsic profile). The combination of both effects is usually achieved in terms of a convolution integral of the intrinsic surface profile with a probability kernel which describes the displacement caused by capillary waves. The main result is that the quadratic measures for the intrinsic and the capillary wave surface width just add up to the square of the so-called "apparent" surface width.

The intrinsic behavior has been dealt with using self-consistent field theory and its extensions [21]. The results show that the density profile over the surface may well be fitted to a function of the form

$$\rho(z) = \frac{\rho_0}{2}\left(1 + \tanh\frac{z}{w_0}\right) , \tag{4}$$

where ρ_0 is the bulk density. In terms if the Flory-Huggins parameter χ and the effective bond length b, the intrinsic surface width is calculated as

$$w_0 = \frac{b}{\sqrt{6\chi}}\,, \tag{5}$$

and for the surface tension, one obtains

$$\gamma = \frac{k_B T}{b^2}\sqrt{\frac{\chi}{6}}\,. \tag{6}$$

For the Flory-Huggins parameter χ, which is a dimensionless measure of the cost in energy to remove a monomer from the bulk, one may employ the mean field estimate

$$\chi = z_{\rm eff}\frac{\epsilon}{k_B T} = \frac{z_{\rm eff}}{T^*} \sim \frac{1}{T^*}\,, \tag{7}$$

where $z_{\rm eff}$ is the effective coordination number of a monomer in the bulk, ϵ is the Lennard-Jones energy, and $T^* = T/(\epsilon/k_B)$ is the dimensionless temperature (see above). Using this mean field estimate, one gets the scaling relations

$$w_0 \sim \sqrt{T^*}\,, \qquad \gamma \sim \frac{1}{\sqrt{T^*}}\,. \tag{8}$$

In order to derive the main results of capillary wave theory [22], let the surface be described in terms of a height function $z = h(x, y)$ over a two-dimensional domain A in the xy-plane. Without loss of generality we use a coordinate system in which the area average of h is zero, $\overline{h} = (1/A)\int\int dxdy\, h(x, y) = 0$. In other words, the function h measures deviations from a flat planar surface. The free energy of the surface is given by

$$W = \int_A \gamma dA\,, \tag{9}$$

where γ denotes the surface tension. In linear approximation for the surface element dA, we get

$$W = \gamma A + \frac{\gamma}{2}\int\int dxdy\, \left[\left(\frac{\partial h}{\partial x}\right)^2 + \left(\frac{\partial h}{\partial y}\right)^2\right]\,. \tag{10}$$

Now assume that we sample the surface using a grid and hence we know the values of h at the discrete points (x_i, y_j), where $i = 1 \ldots N_x$ and $j = 1 \ldots N_y$. We can then represent h by a Fourier series,

$$h(\vec{x}) = \sum_{n_x=-N_x/2}^{N_x/2} \sum_{n_y=-N_y/2}^{N_y/2} a(\vec{q}) \exp i\vec{q}\cdot\vec{x}\,, \tag{11}$$

with wave numbers $q_x = 2\pi n_x/N_x$, $q_y = 2\pi n_y/N_y$, and complex Fourier coefficients $a(\vec{q})$. Using this representation, we find for the surface energy

$$W = \gamma A + \frac{1}{2} \sum_{n_x=-N_x/2}^{N_x/2} \sum_{n_y=-N_y/2}^{N_y/2} |a(\vec{q})|^2 |\vec{q}|^2\,. \tag{12}$$

In Fourier space, the expression for the area average of h^2 (which is a measure for the surface fluctuation, i.e. for the apparent thickness of the surface due to capillary waves of all wave numbers $\vec{q}$) is

$$\overline{h^2} = \frac{1}{A}\int\int dxdy\, h^2(x,y) = \sum_{n_x=-N_x/2}^{N_x/2} \sum_{n_y=-N_y/2}^{N_y/2} |a(\vec{q})|^2\,. \tag{13}$$

According to Eqn. (12), the free energy W is quadratic in the Fourier components $a(\vec{q})$. Hence the Boltzmann factor $\exp(-W/k_BT)$ is of Gaussian form, and for the fluctuation spectrum in Fourier space we can read off the result

$$\langle |a(\vec{q})|^2 \rangle = \frac{k_BT}{\gamma A}\frac{1}{|\vec{q}|^2}\,, \tag{14}$$

where $\langle \ldots \rangle$ denotes averaging with respect to the Boltzmann weight. Inserting this into Eqn. (13), we obtain the following expression for the surface fluctuation:

$$\langle \overline{h^2} \rangle = \frac{k_BT}{\gamma A} \sum_{n_x=-N_x/2}^{N_x/2} \sum_{n_y=-N_y/2}^{N_y/2} \frac{1}{|\vec{q}|^2}\,. \tag{15}$$

On a grid used to sample the surface, this may be calculated numerically as

$$\langle \overline{h^2} \rangle_{\rm grid} = \frac{k_BT}{4\pi^2\gamma}\frac{1}{N_xN_y} \sum_{n_x=-N_x/2}^{N_x/2} \sum_{n_y=-N_y/2}^{N_y/2} \frac{1}{(n_x/N_x)^2 + (n_y/N_y)^2}\,, \tag{16}$$

whereas (replacing sums by integrals) the analytic approximation is

$$\langle \overline{h^2} \rangle_{\rm cont} = \frac{k_BT}{2\pi\gamma} \ln\frac{L}{2a}\,. \tag{17}$$

Here L is the extension of the surface in the lateral directions and may, if necessary, be approximated by the geometric mean $L = (L_xL_y)^{(1/2)}$ (where L_x and L_y differ at most, say,

by a factor of 4). Note that using the geometric mean, $L^2 = L_x L_y = A$ remains the area on which capillary waves may develop and in this manner the arithmetic mean of logarithms, $\ln L = (1/2)(\ln L_x + \ln L_y)$, enters Eqn. (17). In the current derivation, a is the grid spacing, but more generally, $2a$ is the microscopic cutoff for this continuum theory (and, accordingly, π/a is the upper cutoff in wave number space). Usually, Eqn. (17) is written as

$$s^2 \equiv \langle \overline{h^2} \rangle_{\rm cont} = \frac{k_B T}{2\pi\gamma} \ln \frac{q_{\rm max}}{q_{\rm min}} = \frac{k_B T}{2\pi\gamma} \ln \frac{L}{l} \,, \tag{18}$$

where the microscopic cutoff length l depends on the lateral correlation length $\xi_{||}$ [11]).

To determine $\xi_{||}$ we have to explicitly consider the potential $V(h)$ exerted by the surfaces on each other [23,24]

$$\mathcal{H}(h(x,y)) = \int dxdy \left[\left(\frac{\partial h}{\partial x} \right)^2 + \left(\frac{\partial h}{\partial y} \right)^2 \right] + a(T) \left(\exp\left(-\kappa z\right) + \exp\left(-\kappa \left(D - z\right)\right) \right) \tag{19}$$

$$= \int dxdy \left[\left(\frac{\partial h}{\partial x} \right)^2 + \left(\frac{\partial h}{\partial y} \right)^2 \right] + 2a(T) \exp\left(-\frac{\kappa D}{2}\right) \cosh\left(\kappa h\right) \tag{20}$$

with the average film thickness D and the constant κ, which matches in mean field theory of critical wetting with the inverse bulk correlation length ξ_b. Applying a quadratic expansion to the second term of Eqn.(19) we see the formal analogy to the treatment of correlations in standard Ginzburg-Landau theory and hence the correlation length $\xi_{||}$ of $\langle hh' \rangle$ is obtained by [25]

$$\xi_{||}^{-2} = \frac{2a(T)\kappa^2}{\gamma} \exp\left(-\frac{\kappa D}{2}\right) \tag{21}$$

– To summarize, capillary wave theory in harmonic approximation predicts via Eqns. (17) or (18) the logarithmic growth of the surface thickness with surface size and additional the geometrical constraint of the film broads the surface thickness linearly with the film thickness via Eq.(21).

Intrinsic and capillary wave surface broadening can be combined by use of a convolution integral.The result of such a calculation yields a simple method to analyze the simulation data: Fit the surface profile (naively) to a function of the form

$$\rho(z) = \frac{\rho_0}{2}\left(1 + \tanh\frac{z}{w}\right) . \tag{22}$$

Then the square of the apparent surface width w,

$$w^2 = w_0^2 + \frac{\pi}{2}s^2 = w_0^2 + \frac{k_BT}{4\gamma}\ln L + \frac{k_BT}{16\gamma}\kappa D + const. \tag{23}$$

is the sum of squares of the intrinsic, capillary wave contributions and the film fluctuations, whereas *const.* compromises the constant terms of the latter one.

RESULTS

In Fig. 3, the validity of the free energy functional $W[a(q)]$ according to Eqn. (12) is tested. The Boltzmann factor $\exp(-W[a(q)]/k_BT)$ predicts Gaussian statistics for the Fourier amplitudes $a(q)$. This is confirmed by the figure. We can therefore try to exploit the relation (14) between the fluctuation $\langle|a(q)|^2\rangle$ of the Fourier coefficients and the surface tension γ. This is done in Fig. 4. In this plot, results for chain length $N = 120$ and temperature $T^* = 6$, obtained in simulations of varying system size, are combined. For increasing wave number q, we find that in our simulations the fluctuations $\langle|a(q)|^2\rangle$ decay too slowly, and only next to $q = 0$ a linear fit, as predicted by the Gaussian theory, is possible. Best we can do is therefore to extract the value for γ in the low wave number limit ($q \to 0$), which is found to be $\gamma \approx 1.3$ (in physical units, this corresponds to around $7.5 \cdot 10^{-3}$ N/m or dyne/cm, see Tab. I). It is noteworthy that at least 300 000 MD steps must be computed to get some useful result for the Fourier coefficient with $q = 2\pi/32$, and 700 000 MD steps are necessary to reduce the statistical inaccuracy of the Fourier coefficients to below 10%.

We now turn to the apparent surface width and its dependence on the system size. Fig. 5 demonstrates that a fit according to Eqn. (22) is appropriate. In Fig. 6 then, we exploit Eqn. (23) in the form

$$a_0 = w_0^2 - \frac{k_BT}{16\gamma}\kappa D - const. \qquad \text{and} \qquad a_1 = \frac{k_BT}{4\gamma} , \tag{24}$$

where a_0 and a_1 have to be determined by fitting linearly,

$$w^2 = a_0 + \frac{1}{2} a_1 \ln(L_x L_y) \,. \tag{25}$$

From the slope a_1 we obtain another estimate for the surface tension γ which is independent from the one obtained via the fluctuation spectrum (no Fourier transform is necessary). However, best we can get from the figure is $\gamma \approx 1.47$, which is 12% higher than the fluctuation value (Fig. 4).

The data computed with the smallest system length (L=16) is rather to small to get reliable results (Fig. 4,6). The reason could be either the ratio of the intrinsic structure or the correlation length $\xi_{||}$ to lateral system size is not small enough. Therefore we calculate the transverse length scale κ^{-1} by increasing the film thickness D (Eqn. (7)). We obtain a linear dependance $w^2 \propto D$ with a strong correlation of the fluctuations of the surfaces ($\kappa^{-1} = 67 \pm 10$). The correlation length is an order of magnitude larger than the correlation length in bulk ($\xi_b = 1.3$) or the gyration radius ($R_g = 4.1$). As mentioned above in critical wetting theory κ^{-1} is proposed to be the correlation length of concentration fluctuations in the bulk [23] or half of the intrinsic width [11]. This seems to be not applicable to free standing thin films with no confining walls. In the case of $L < \xi_{||}$ the theory of capillary wave fluctuations is not applicable. For that case the whole film oszillates and we expect w^2 becomes independant from the film thickness. Therefore we can conclude that for the considered system sizes $\xi_{||} < L$ is valid.

Up to this point, all results reported are for the temperature $T^* = 6$ ($T = 361$K), but additional simulations were performed to investigate the temperature dependence of the surface width. The range of temperatures we studied, $T^* = 6 - 10$ ($T = 361 - 601$K), lies above the glass transition temperature [15]. Flory's mean field theory of polymer solutions applied to the melt-gas system predicts a shape of the coexistence curve as sketched in Fig. 8. To get an estimate for the Θ-temperature, we plotted in Fig. 9 the bulk density vs. the temperature. A linear extrapolation of the binodal line, i.e. the limit $N \to \infty$, yields $\Theta = 18.5 \pm 0.1$. Thus even with the higher simulation temperatures we do not approach

criticality.

The self-consistent field theory applied to polymer interfaces [21], the predictions for the surface tensions are $\gamma \sim 1/\sqrt{T^*}$ (Eqn. (8)) and together with Eqn. (23) we expect $w^2 \sim T^{1.5}$. In Fig. 10, however, we see a steeper increase of the surface width with growing temperature. But we have not taken into account an explict temperature dependance of κD. Additionally the temperature dependance of the lateral correlation length has to consider and therefore an eventual change of the applied theory.

ACKNOWLEDGMENTS

The authors gratefully acknowledge the support from the Bundesministerium für Bildung und Forschung (BMBF) in the framework of the project "Computersimulation komplexer Materialien" under grant no. 03N8008D. Part of the computer simulation has been performed using the facilities at the IWR of the University of Heidelberg. We again thank our former colleague Andreas Linke to whom essential parts of our simulation code must be contributed.

REFERENCES

[1] J. Stecki and S. Toxvaerd, J. Chem. Phys. **103**, 4352 (1995).

[2] B. Smit, Phys. Rev. A **37**, 3431 (1988).

[3] S. Enders, B. A. Wolf, and K. Binder, J. Chem. Phys. **109**, 3811 (1995).

[4] G. J. A. Ypma, P. Cifra, E. Nies, and A. R. D. van Bergen, Macromolecules **29**, 1252 (1996).

[5] R. B. Pandey, A. Milchev, and K. Binder, Macromolecules **30**, 1194 (1997).

[6] R. H. Fowler, Proc. Roy. Soc. London, Ser. A **159**, 229 (1937).

[7] J. G. Kirkwood and F. P. Buff, J. Chem. Phys. **17**, 338 (1949).

[8] M. Meyer, M. Mareschal, and M. Hayoun, J. Chem. Phys. **89**, 1067 (1988).

[9] J. K. Lee, J. A. Barker, and G. M. Pound, J. Chem. Phys. **60**, 1976 (1974).

[10] J. A. Barker and D. Henderson, Rev. Mod. Phys. **48**, 587 (76).

[11] A. Werner, F. Schmid, M. Müller, and K. Binder, J. Chem. Phys. (to be published).

[12] M. Müller and A. Werner, J. Chem. Phys. (to be published).

[13] I. Carmesin and K. Kremer, Macromolecules **21**, 2819 (1988).

[14] M. P. Allen and D. J. Tildesley, *Computer Simulation of Liquids* (Clarendon Press, Oxford, 1987).

[15] D. Rigby and R. Roe, J. Chem. Phys. **87**, 7285 (1987).

[16] W. Paul, D. Y. Yoon, and G. D. Smith, J. Chem. Phys. **103**, 1702 (1995).

[17] G. Pätzold, T. Hapke, A. Linke, and D. W. Heermann, Thin Solid Films **295**, 199 (1997).

[18] T. Hapke, A. Linke, G. Pätzold, and D. W. Heermann, Surf. Sci. **373**, 109 (1997).

[19] T. Hapke, Simulation mikromechanischer Eigenschaften von amorphen makromolekularen Gläsern am Beispiel von Polyethylen, Diplomarbeit am Institut für Theoretische Physik der Universität Heidelberg, 1995 (unpublished).

[20] R. Sedgewick, in *Algorithms in C++* (Addison-Wesley, Reading/Massachusetts, 1992), Chap. 28.

[21] E. Helfand and Y. Tagami, J. Chem. Phys. **56**, 3592 (1972).

[22] F. P. Buff, R. A. Lovett, and F. H. Stillinger Jr., Phys. Rev. Lett. **15**, 621 (1965).

[23] A. O. Parray and R. Evans, Physica A **181**, 250 (1992).

[24] K. Binder, R. Evans, D. P. Landau, and A. M. Ferrenberg, Phys. Rev. E **53**, 5023 (1996).

[25] J. J. Binney, N. J. Dowrick, A. J. Fisher, and M. E. J. Newman, in *The Theory of Critical Phenomena* (Clarendon Press, Oxford, 1992), Chap. 8.

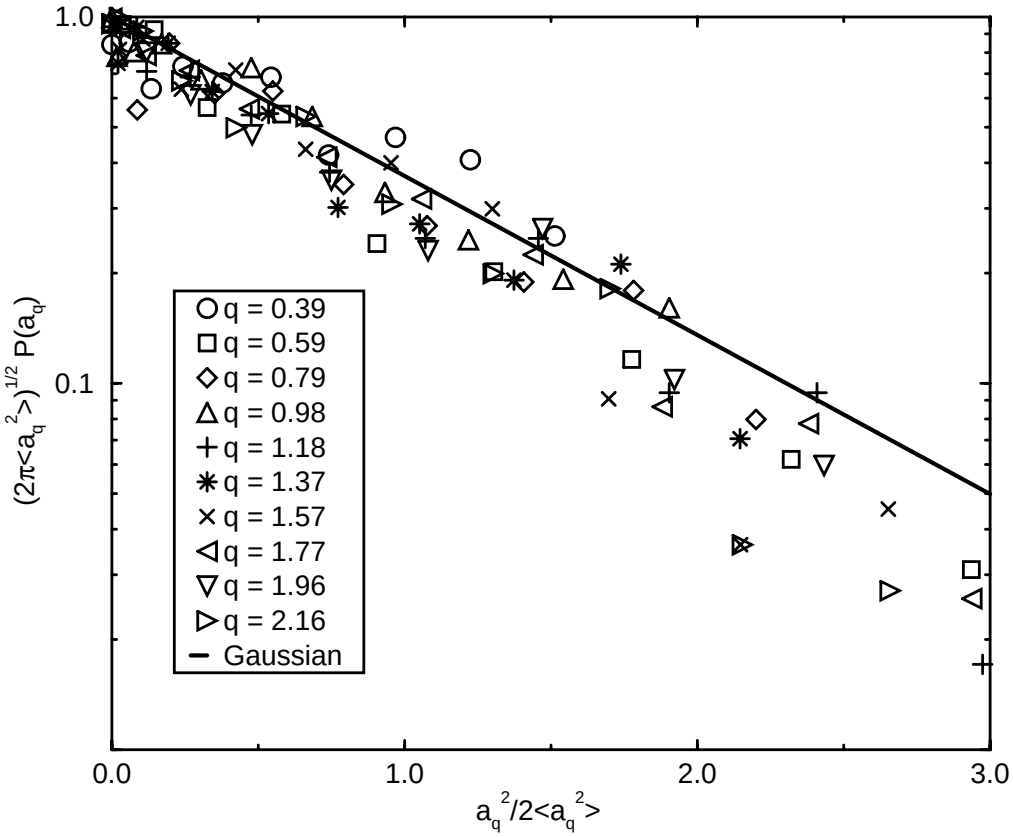

FIG. 3. Probability distribution $P(a_q)$ of the Fourier components a_q for wave vectors of different magnitude q. The solid line marks the expected Gaussian behavior.

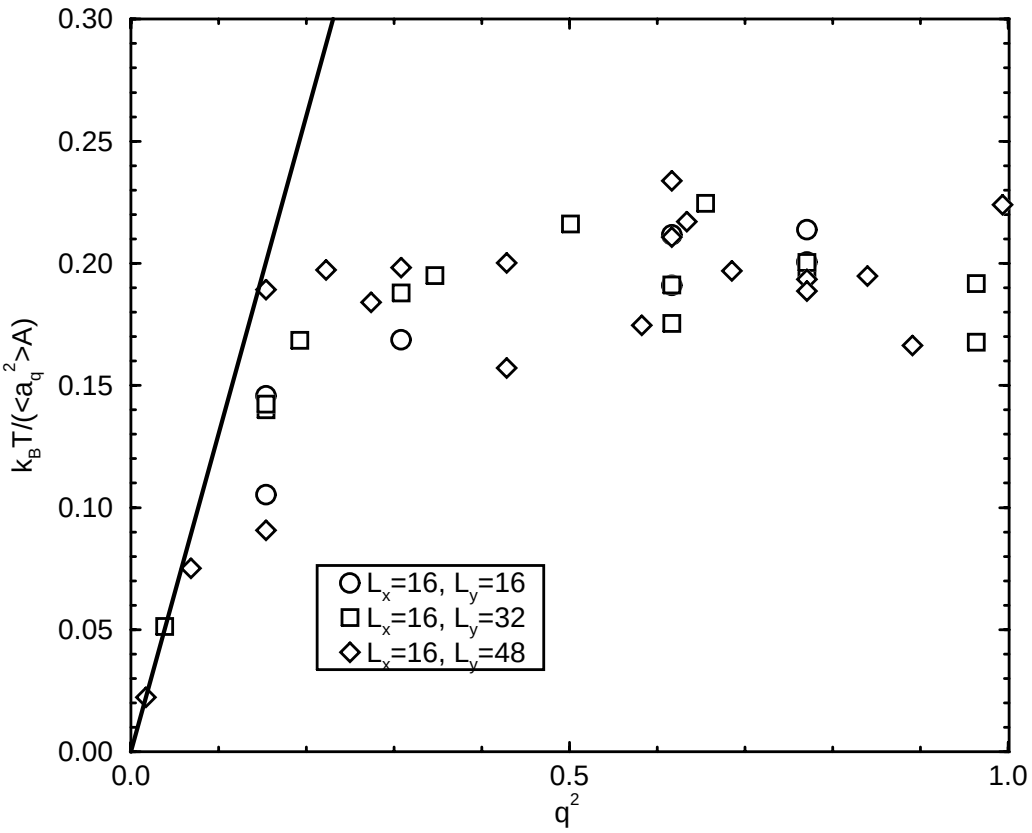

FIG. 4. Determination of the surface tension γ from the fluctuation of Fourier amplitudes $\langle a_q^2 \rangle$ for different wave numbers q. According to simple capillary wave theory, one should see a straight line with slope γ. We find, however, that the surface tension is systematically underestimated for increasing wave number. From the figure, we get fit the estimate $\gamma \to 1.3$ for $q \to 0$ (solid line).

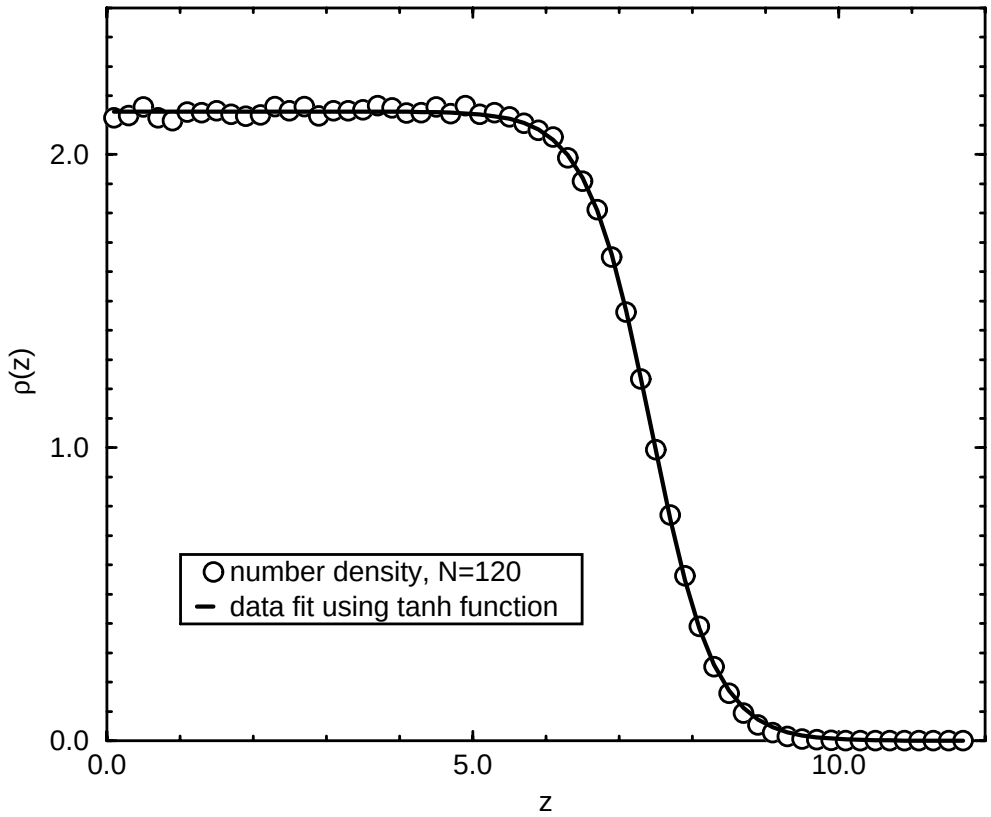

FIG. 5. Average profile $\rho(z)$ of the monomer number density and data fit based on a tanh function. The chain length is $N = 120$ and the reduced temperature $T^* = 6$. In the reduced length scale used in the figure, 1 unit corresponds to 3.8 Å.

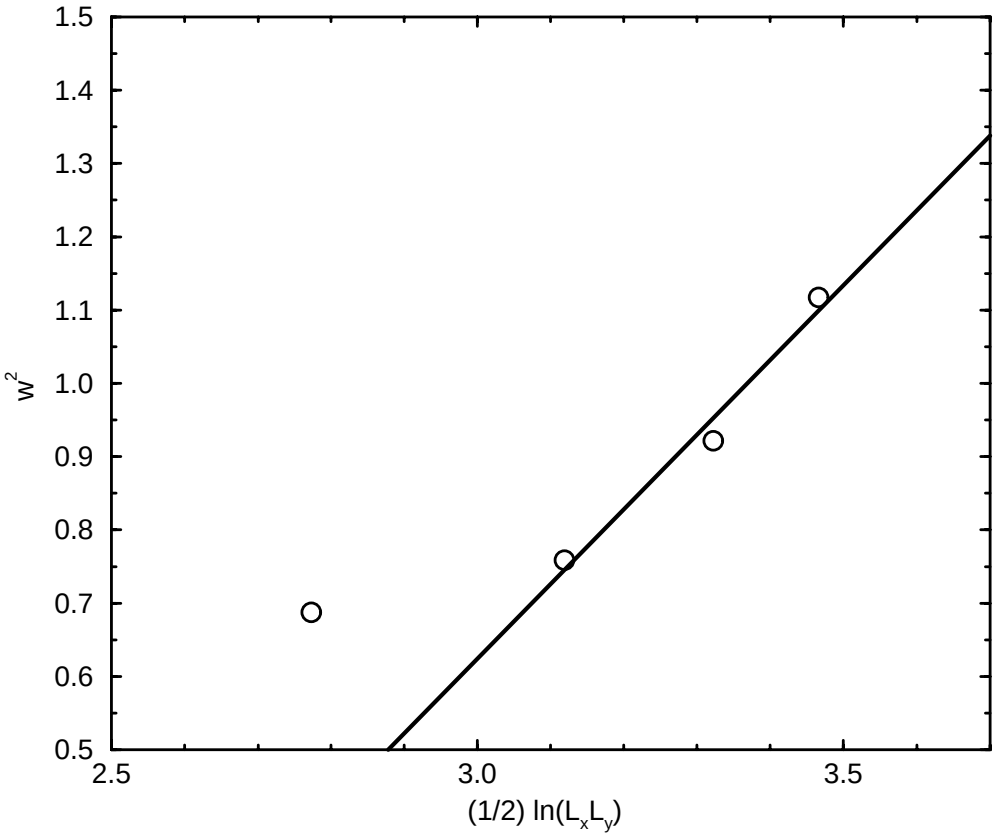

FIG. 6. The square of the apparent surface width w vs. half the logarithm of the surface area. To obtain the surface width, the density profile $\rho(z)$ has been sampled in 100 data bins. In theory, the data points should lie on a straight line whose slope is inversely proportional to the surface tension γ. Based on the three points for the larger systems only, the estimate is $\gamma \approx 1.47$.

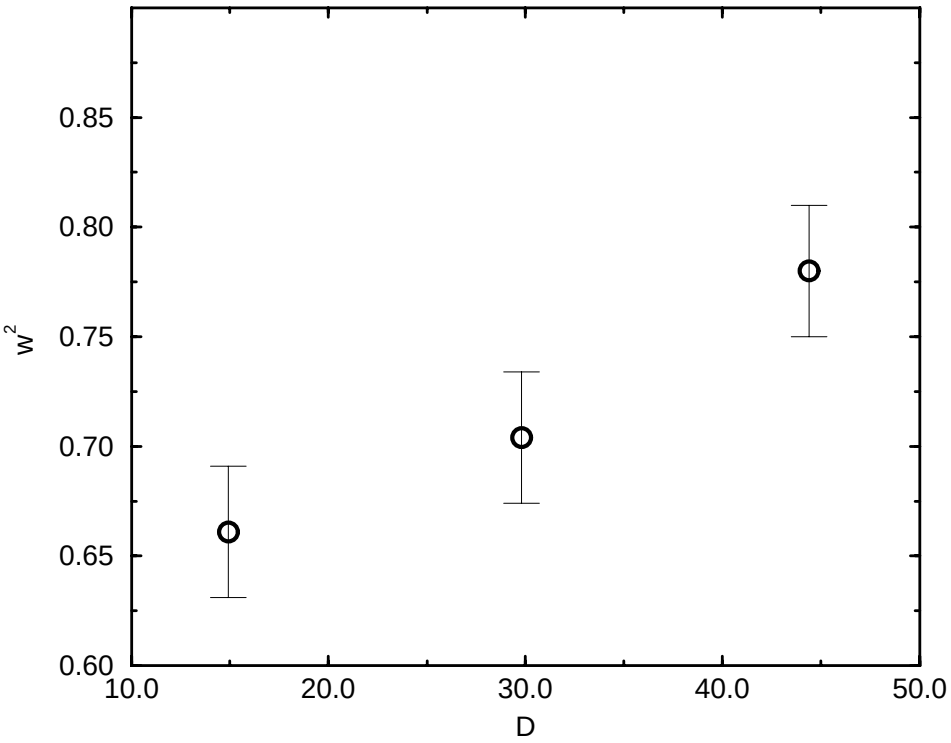

FIG. 7. The square of the apparent surface widht w^2 vs. the film thickness D. In the regime $L > \xi_{||}$ the theory of the capillary wave fluctuations predicts a linear dependance whereas for $L < \xi_{||}$ we expect w becomes independant from the film thickness

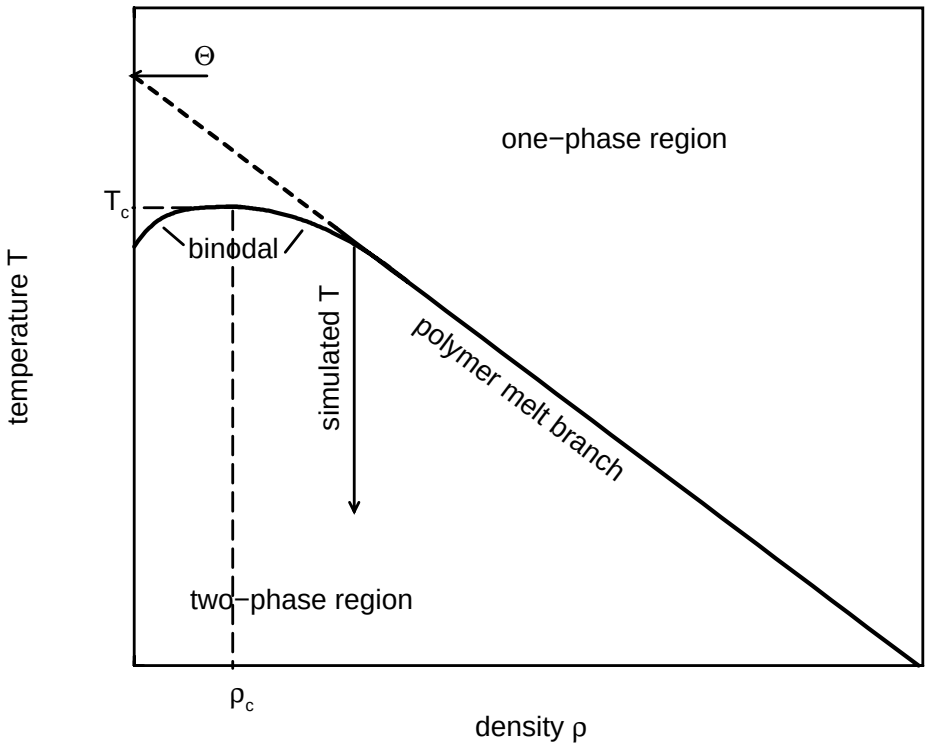

FIG. 8. Schematic phase diagram of a polymer-vacuum system in the space of temperature T and the polymer bulk density ρ. The coexistence curve (binodal line) separates a polymer melt with overlapping chains from a gaseous phase with collapsed chains. These two branches of the coexistence curve merge at a critical point T_c, ϕ_c. For $N \to \infty$ the critical point merges with the Θ-point (dotted line).

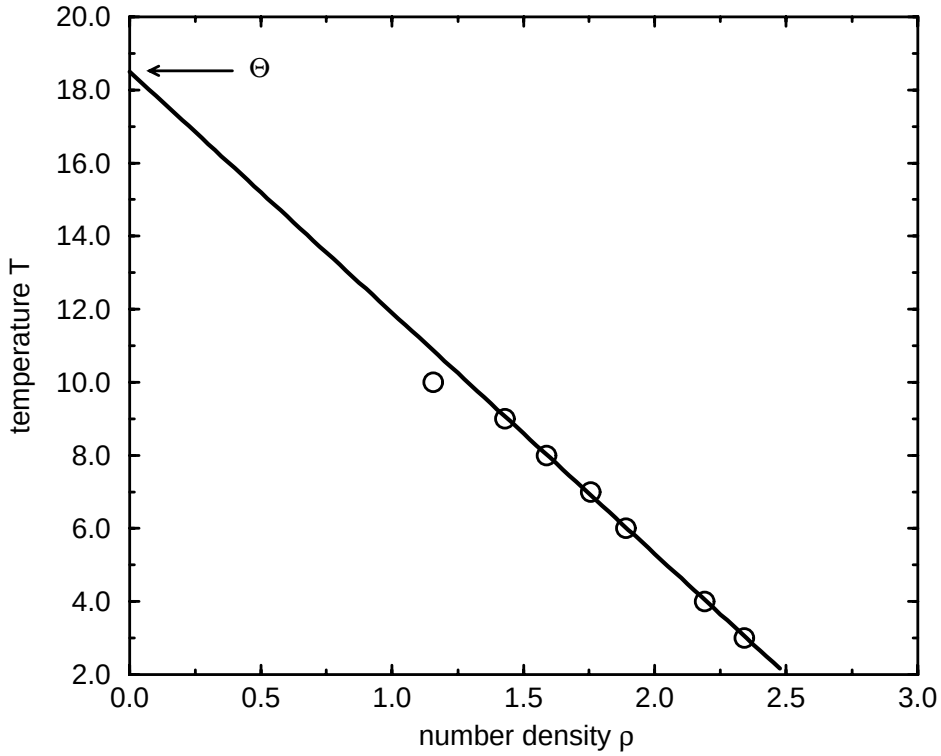

FIG. 9. Gas-melt coexistence curve as determined from simulations of free standing polymer films for varying temperature. For the Θ-temperature one finds by linear extrapolation $\Theta \approx 18.5$.

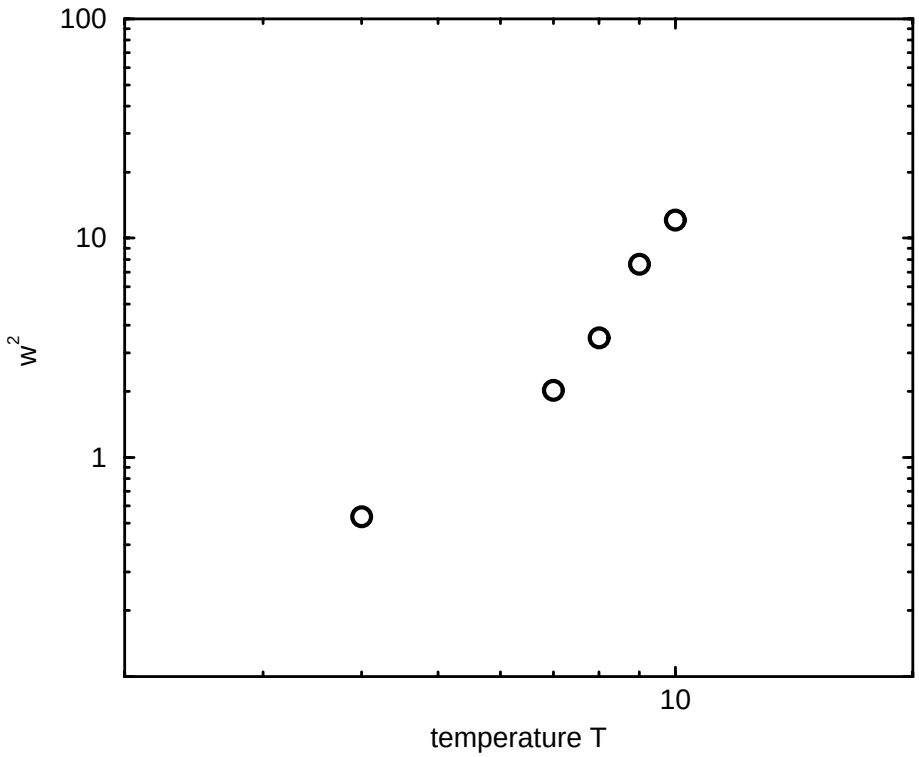

FIG. 10. Dependence of the surface width on the temperature.

TABLES

TABLE I. Parameters of the polyethylene model.

Lennard–Jones energy, ϵ	$8.3027 \cdot 10^{-22}$ J	5.18 meV
Lennard–Jones length, σ	380 pm	3.8 Å
monomer mass (CH_2 group), m	$2.3248 \cdot 10^{-26}$ kg	14 atomic units
unit of temperature, ϵ/k_B	60.1357 K	
unit of mass density, m/σ^3	423.6687 kg/m^3	0.4237 g/cm^3
unit of time, $(m\sigma^2/\epsilon)^{1/2}$	2.0108 ps	
unit of velocity, $(\epsilon/m)^{1/2}$	188.9822 m/s	
unit of force, ϵ/σ	2.1849 pN	1.36 meV/Å
unit of spring constant, ϵ/σ^2	$5.7498 \cdot 10^{-3}$ N/m	0.36 meV/Å^2
unit of pressure, ϵ/σ^3	151.3103 bar	0.09 meV/Å^3
unit of surface tension, ϵ/σ^2	$5.75 \cdot 10^{-3}$ N/m	
temperature, T	361 K	
bond length, l_0	152 pm	1.52 Å
bond angle, θ_0	109.47°	$\cos\theta_0 = -1/3$
spring constant (bond length), k_b	$5.7498 \cdot 10^{1}$ N/m	3.59 eV/Å^2
bending constant (bond angle), k_θ	$8.3027 \cdot 10^{-19}$ J	5.18 eV
simulation time step, Δt	2.0108 fs	

TABLE II. Computational time per particle and molecular dynamics step.

number of particles (monomers)	8 160	16 320	24 480
box dimension, $L_x \times L_y \times L_z$ [scaled units]	$16 \times 40 \times 16$	$16 \times 32 \times 40$	$16 \times 48 \times 40$
computational time [ms]	0.521	0.529	0.489